Swapping Autoencoder for Deep Image Manipulation

Taesung Park[12]   **Jun-Yan Zhu**[23]   **Oliver Wang**[2]   **Jingwan Lu**[2]

Eli Shechtman[2]   **Alexei A. Efros**[12]   **Richard Zhang**[2]

[1]UC Berkeley   [2]Adobe Research   [3]CMU

Abstract

Deep generative models have become increasingly effective at producing realistic images from randomly sampled seeds, but using such models for *controllable manipulation of existing images* remains challenging. We propose the Swapping Autoencoder, a deep model designed specifically for image manipulation, rather than random sampling. The key idea is to encode an image into two independent components and enforce that any swapped combination maps to a realistic image. In particular, we encourage the components to represent structure and texture, by enforcing one component to encode co-occurrent patch statistics across different parts of the image. As our method is trained with an encoder, finding the latent codes for a new input image becomes trivial, rather than cumbersome. As a result, our method enables us to manipulate real input images in various ways, including texture swapping, local and global editing, and latent code vector arithmetic. Experiments on multiple datasets show that our model produces better results and is substantially more efficient compared to recent generative models.

input   texture swapping
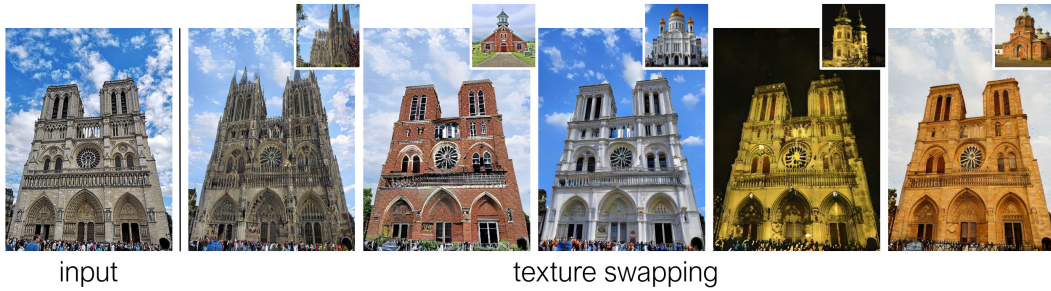
Figure 1: Our Swapping Autoencoder learns to disentangle texture from structure for image editing tasks. One such task is texture swapping, shown here. Please see our project webpage for a demo video of our editing method.

1   Introduction

Traditional photo-editing tools, such as Photoshop, operate solely within the confines of the input image, i.e. they can only "recycle" the pixels that are already there. The promise of using machine learning for image manipulation has been to incorporate the *generic visual knowledge* drawn from external visual datasets into the editing process. The aim is to enable new class of editing operations, such as inpainting large image regions [65, 87, 58], synthesizing photorealistic images from layouts [35, 79, 64], replacing objects [95, 29], or changing the time photo is taken [43, 2].

However, learning-driven image manipulation brings in its own challenges. For image editing, there is a fundamental conflict: what information should be gleaned from the dataset versus information that must be retained from the input image? If the output image relies too much on the dataset, it will retain no resemblance to the input, so can hardly be called "editing", whereas relying too much on the input lessens the value of the dataset. This conflict can be viewed as a disentanglement

problem. Starting from image pixels, one needs to factor out the visual information which is specific to a given image from information that is applicable across different images of the dataset. Indeed, many existing works on learning-based image manipulation, though not always explicitly framed as learning disentanglement, end up doing so, using paired supervision [75, 35, 79, 64], domain supervision [95, 31, 59, 2], or inductive bias of the model architecture [1, 21].

In our work, we aim to discover a disentanglement suitable for image editing in an *unsupervised setting*. We argue that it is natural to explicitly factor out the visual patterns within the image that must change consistently with respect to each other. We operationalize this by learning an autoencoder with two modular latent codes, one to capture the *within-image visual patterns*, and another to capture the rest of the information. We enforce that any arbitrary combination of these codes map to a realistic image. To disentangle these two factors, we ensure that all image patches with the same within-image code appear coherent with each other. Interestingly, this coincides with the classic definition of visual texture in a line of works started by Julesz [40, 42, 41, 69, 24, 17, 57]. The second code captures the remaining information, coinciding with structure. As such, we refer to the two codes as *texture* and *structure* codes.

A natural question to ask is: why not simply use unconditional GANs [19] that have been shown to disentangle style and content in unsupervised settings [45, 46, 21]? The short answer is that these methods do not work well for editing *existing* images. Unconditional GANs learn a mapping from an easy-to-sample (typically Gaussian) distribution. Some methods [4, 1, 46] have been suggested to *retrofit* pre-trained unconditional GAN models to find the latent vector that reproduces the input image, but we show that these methods are inaccurate and magnitudes slower than our method. The conditional GAN models [35, 95, 31, 64] address this problem by starting with input images, but they require the task to be defined *a priori*. In contrast, our model learns an embedding space that is useful for image manipulation in several downstream tasks, including synthesizing new image hybrids (see Figure 1), smooth manipulation of attributes or domain transfer by traversing latent directions (Figure 7), and local manipulation of the scene structure (Figure 8).

To show the effectiveness of our method, we evaluate it on multiple datasets, such as LSUN churches and bedrooms [86], FlickrFaces-HQ [45], and newly collected datasets of mountains and waterfalls, using both automatic metrics and human perceptual judgments. We also present an interactive UI (please see our video in the project webpage) that showcases the advantages of our method.

2 Related Work

Conditional generative models, such as image-to-image translation [35, 95], learn to directly synthesize an output image given a user input. Many applications have been successfully built with this framework, including image inpainting [65, 33, 83, 58], photo colorization [90, 53, 92, 23], texture and geometry synthesis [93, 20, 81], sketch2photo [71], semantic image synthesis and editing [79, 68, 10, 64]. Recent methods extent it to multi-domain and multi-modal setting [31, 96, 59, 88, 12]. However, it is challenging to apply such methods to on-the-fly image manipulation, because for each new application and new user input, a new model needs to be trained. We present a framework for both image synthesis and manipulation, in which the task can be defined by one or a small number of examples at run-time. While recent works [72, 73] propose to learn a single-image GANs for image editing, our model can be quickly applied to a test image without extensive computation of single-image training.

Deep image editing via latent space exploration modifies the latent vector of a pre-trained, unconditional generative model (e.g., a GAN [19]) according to the desired user edits. For example, iGAN [94] obtains the latent code using an encoder-based initialization followed by Quasi-Newton optimization, and updates the code according to new user constraints. Similar ideas have been explored in other tasks like image inpainting, face editing, and deblurring [8, 66, 84, 3]. More recently, instead of using the input latent space, GANPaint [4] adapts layers of a pre-trained GAN for each input image and updates layers according to a user's semantic control [5]. Image2StyleGAN [1] and StyleGAN2 [46] reconstruct the image using an extended embedding space and noise vectors. Our work differs in that we allow the code space to be learned rather than sampled from a fixed distribution, thus making it much more flexible. In addition, we train an encoder together with the generator, which allows for significantly faster reconstruction.

Disentanglement of content and style generative models. Deep generative models learn to model the data distribution of natural images [70, 19, 50, 13, 11, 82], many of which aim to represent content and style as independently controllable factors [45, 46, 47, 15, 80]. Of special relevance to our work are models that use code swapping during training [62, 30, 38, 74, 15, 45]. Our work differs from them

in three aspects. First, while most require human supervision, such as class labels [62], pairwise image similarity [38], images pairs with same appearances [15], or object locations [74], our method is fully unsupervised. Second, our decomposable structure and texture codes allow each factor be extracted from the input images to control different aspects of the image, and produce higher-quality results when mixed. Note that for our application, image quality and flexible control are critically important, as we focus on image manipulation rather than unsupervised feature learning. Recent image-to-image translation methods also use code swapping but require ground truth domain labels [52, 54, 56]. In concurrent work, Anokhin et al. [2] and ALAE [67] propose models very close to our code swapping scheme for image editing purposes.

Style transfer. Modeling style and content is a classic computer vision and graphics problem [75, 25]. Several recent works revisited the topic using modern neural networks [18, 39, 76, 9], by measuring content using perceptual distance [18, 14], and style as global texture statistics, e.g., a Gram matrix. These methods can transfer low-level styles such as brush strokes, but often fail to capture larger scale semantic structures. Photorealistic style transfer methods further constrain the result to be represented by local affine color transforms from the input image [61, 55, 85], but such methods only allow local color changes. In contrast, our learned decomposition can transfer semantically meaningful structure, such as the architectural details of a church, as well as perform other image editing operations.

3 Method

What is the desired representation for image editing? We argue that such representation should be able to reconstruct the input image easily and precisely. Each code in the representation can be independently modified such that the resulting image both looks realistic and reflects the unmodified codes. The representation should also support both global and local image editing.

To achieve the above goals, we train a swapping autoencoder (shown in Figure 2) consisting of an encoder E and a generator G, with the core objectives of 1) accurately reconstructing an image, 2) learning independent components that can be mixed to create a new hybrid image, and 3) disentangling texture from structure by using a patch discriminator that learns co-occurrence statistics of image patches.

3.1 Accurate and realistic reconstruction

In a classic autoencoder [28], the encoder E and generator G form a mapping between image $\mathbf{x} \sim \mathbf{X} \subset \mathbb{R}^{H \times W \times 3}$ and latent code $\mathbf{z} \sim \mathbf{Z}$. As seen in the top branch of Figure 2, our autoencoder also follows this framework, using an image reconstruction loss:

$$\mathcal{L}_{\text{rec}}(E, G) = \mathbb{E}_{\mathbf{x} \sim \mathbf{X}}[\|\mathbf{x} - G(E(\mathbf{x}))\|_1]. \tag{1}$$

In addition, we wish for the image to be realistic, enforced by a discriminator D. The non-saturating adversarial loss [19] for the generator G and encoder E is calculated as:

$$\mathcal{L}_{\text{GAN,rec}}(E, G, D) = \mathbb{E}_{\mathbf{x} \sim \mathbf{X}}[-\log(D(G(E(\mathbf{x}))))]. \tag{2}$$

3.2 Decomposable latent codes

We divide the latent space $\mathbf{Z}$ into two components, $\mathbf{z} = (\mathbf{z}_s, \mathbf{z}_t)$, and enforce that swapping components with those from other images still produces realistic images, using the GAN loss [19].

$$\mathcal{L}_{\text{GAN,swap}}(E, G, D) = \mathbb{E}_{\mathbf{x}^1, \mathbf{x}^2 \sim \mathbf{X}, \mathbf{x}^1 \neq \mathbf{x}^2}\left[-\log(D(G(\mathbf{z}_s^1, \mathbf{z}_t^2)))\right], \tag{3}$$

where $\mathbf{z}_s^1$, $\mathbf{z}_t^2$ are the first and second components of $E(\mathbf{x}^1)$, $E(\mathbf{x}^2)$, respectively. Furthermore, as shown in Figure 2, we design the shapes of $\mathbf{z}_s$ and $\mathbf{z}_t$ asymmetrically such that $\mathbf{z}_s$ is a tensor with spatial dimensions, while $\mathbf{z}_t$ is a vector. In our model, $\mathbf{z}_s$ and $\mathbf{z}_t$ are intended to encode structure and texture information, and hence named *structure* and *texture* code, respectively, for convenience. At each training iteration, we randomly sample two images $\mathbf{x}^1$ and $\mathbf{x}^2$, and enforce $\mathcal{L}_{\text{rec}}$ and $\mathcal{L}_{\text{GAN,rec}}$ on $\mathbf{x}^1$, and $\mathcal{L}_{\text{GAN,swap}}$ on the hybrid image of $\mathbf{x}^1$ and $\mathbf{x}^2$.

A majority of recent deep generative models [6, 27, 13, 11, 48, 45, 46], such as in GANs [19] and VAEs [50], attempt to make the latent space Gaussian to enable random sampling. In contrast, we do not enforce such constraint on the latent space of our model. Our swapping constraint focuses on making the "distribution" around a *specific* input image and its plausible variations well-modeled.
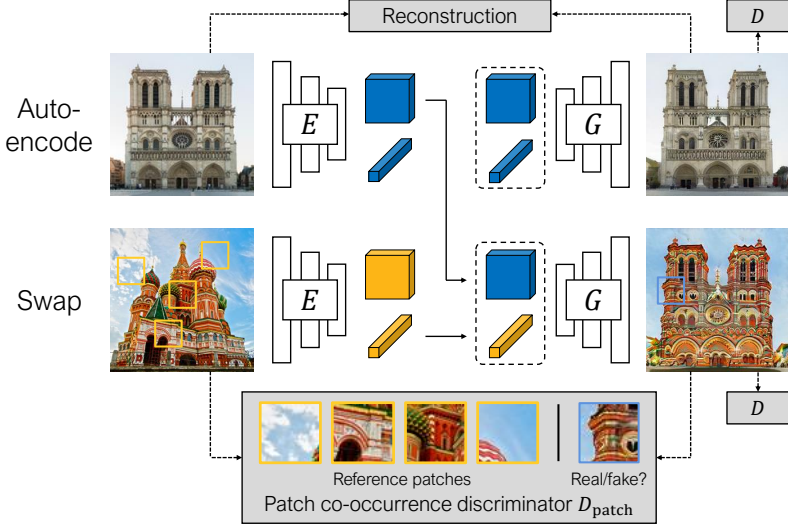
Figure 2: **Swapping Autoencoder** consists of autoencoding (*top*) and swapping (*bottom*) operation. **(Top)** An encoder E embeds an input (Notre-Dame) into two codes. The structure code (▭) is a tensor with spatial dimensions; the texture code (▱) is a 2048-dimensional vector. Decoding with generator G should produce a realistic image (enforced by discriminator D) matching the input (reconstruction loss). **(Bottom)** Decoding with the texture code from a second image (Saint Basil's Cathedral) should look realistic (via D) and match the texture of the image, by training with a patch co-occurrence discriminator D_{patch} that enforces the output and reference patches look indistinguishable.

Under ideal convergence, the training of the Swapping Autoencoder encourages several desirable properties of the learned embedding space $\mathbf{Z}$. First, the encoding function E is optimized toward injection, due to the reconstruction loss, in that different images are mapped to different latent codes. Also, our design choices encourage that different codes produce different outputs via G: the texture code must capture the texture distribution, while the structure code must capture location-specific information of the input images (see Appendix B.1 for more details). Lastly, the joint distribution of the two codes of the swap-generated images is factored by construction, since the structure codes are combined with random texture codes.

3.3 Co-occurrent patch statistics

While the constraints above are sufficient for our swapping autoencoder to learn a factored representation, the resulting representation will not necessarily be intuitive for image editing, with no guarantee that $\mathbf{z}_s$ and $\mathbf{z}_t$ actually represent structure and texture. To address this, we encourage the texture code $\mathbf{z}_t$ to maintain the same texture in any swap-generated images. We introduce a patch co-occurrence discriminator D_{patch}, as shown in the bottom of Figure 2. The generator aims to generate a hybrid image $G(\mathbf{z}_s^1, \mathbf{z}_t^2)$, such that any patch from the hybrid cannot be distinguished from a group of patches from input $\mathbf{x}^2$.

$$\mathcal{L}_{\text{CooccurGAN}}(E, G, D_{\text{patch}}) = \mathbb{E}_{\mathbf{x}^1, \mathbf{x}^2 \sim \mathbf{X}}\left[-\log\left(D_{\text{patch}}\left(\texttt{crop}(G(\mathbf{z}_s^1, \mathbf{z}_t^2)), \texttt{crops}(\mathbf{x}^2)\right)\right)\right], \quad (4)$$

where `crop` selects a random patch of size $1/8$ to $1/4$ of the full image dimension on each side (and `crops` is a collection of multiple patches). Our formulation is inspired by Julesz's theory of texture perception [40, 42] (long used in texture synthesis [69, 17]), which hypothesizes that images with similar marginal and joint feature statistics appear perceptually similar. Our co-occurence discriminator serves to enforce that the joint statistics of a learned representation be consistently transferred. Similar ideas for modeling co-occurences have been used for propagating a single texture in a supervised setting [81], self-supervised representation learning [36], and identifying image composites [32].

3.4 Overall training and architecture

Our final objective function for the encoder and generator is $\mathcal{L}_{\text{total}} = \mathcal{L}_{\text{rec}} + 0.5\mathcal{L}_{\text{GAN,rec}} + 0.5\mathcal{L}_{\text{GAN,swap}} + \mathcal{L}_{\text{CooccurGAN}}$. The discriminator objective and design follows StyleGAN2 [46]. The co-occurrence patch discriminator first extracts features for each patch, and then concatenates them to pass to the final

Method	Runtime (sec) (↓)	LPIPS Reconstruction (↓)			
		Church	FFHQ	Waterfall	Average
Ours	**0.101**	0.227	**0.074**	**0.238**	**0.180**
Im2StyleGAN	495	**0.186**	0.174	0.281	0.214
StyleGAN2	96	0.377	0.215	0.384	0.325

Figure 3: **Embedding examples and reconstruction quality**. We project images into embedding spaces for our method and baseline GAN models, Im2StyleGAN [1, 45] and StyleGAN2 [46]. Our reconstructions better preserve the detailed outline (e.g., doorway, eye gaze) than StyleGAN2, and appear crisper than Im2StyleGAN. This is verified on average with the LPIPS metric [91]. Our method also reconstructs images much faster than recent generative models that use iterative optimization. See Appendix A for more visual examples.

classification layer. The encoder consists of 4 downsampling ResNet [22] blocks to produce the tensor $\mathbf{z}_s$, and a dense layer after average pooling to produce the vector $\mathbf{z}_t$. As a consequence, the structure code $\mathbf{z}_s$, is limited by its receptive field at each location, providing an inductive bias for capturing local information. On the other hand, the texture code $\mathbf{z}_t$, deprived of spatial information by the average pooling, can only process aggregated feature distributions, forming a bias for controlling global style. The generator is based on StyleGAN2, with weights modulated by the texture code. Please see Appendix B.1 for a detailed specification of the architecture, as well as details of the discriminator loss function.

4 Experiments

The proposed method can be used to efficiently embed a given image into a factored latent space, and to generate hybrid images by swapping latent codes. We show that the disentanglement of latent codes into the classic concepts of "style" and "content" is competitive even with style transfer methods that address this specific task [51, 85], while producing more photorealistic results. Furthermore, we observe that even without an explicit objective to encourage it, vector arithmetic in the learned embedding space **Z** leads to consistent and plausible image manipulations [7, 45, 37]. This opens up a powerful set of operations, such as attribute editing, image translation, and interactive image editing, which we explore.

We first describe our experimental setup. We then evaluate our method on: (1) quickly and accurately embedding a test image, (2) producing realistic hybrid images with a factored latent code that corresponds to the concepts of texture and structure, and (3) editability and usefulness of the latent space. We evaluate each aspect separately, with appropriate comparisons to existing methods.

4.1 Experimental setup

Datasets. For existing datasets, our model is trained on LSUN Churches, Bedrooms [86], Animal Faces HQ (AFHQ) [12], Flickr Faces HQ (FFHQ) [45], all at resolution of 256px except FFHQ at 1024px. In addition, we introduce new datasets, which are Portrait2FFHQ, a combined dataset of 17k portrait paintings from `wikiart.org` and FFHQ at 256px, Flickr Mountain, 0.5M mountain images from `flickr.com`, and Waterfall, of 90k 256px waterfall images. Flickr Mountain is trained at 512px resolution, but the model can handle larger image sizes (e.g., 1920×1080) due to the fully convolutional architecture.

Baselines. To use a GAN model for downstream image editing, one must embed the image into its latent space [94]. We compare our approach to two recent solutions. Im2StyleGAN [1] present a method for embedding into StyleGAN [45], using iterative optimization into the "W^+-space" of the model. The StyleGAN2 model [46] also includes an optimization-based method to embed into its latent space and noise vectors. One application of this embedding is producing hybrids. StyleGAN and StyleGAN2 present an emergent hierarchical parameter space that allows hybrids to be produced by mixing parameters of two images. We additionally compare to image stylization methods, which aim to mix the "style" of one image with the "content" from another. STROTSS [51] is an optimization-based framework, in the spirit of the classic method of Gatys et al. [18]. We also compare to WCT^2 [85], a recent state-of-the-art *photorealistic* style transfer method based on a feedforward network.

4.2 Image embedding

The first step of manipulating an image with a generative model is projecting it into its latent spade. If the input image cannot be projected with high fidelity, the embedded vector cannot be used for editing, as the user would be editing a different image. Figure 3 illustrates both example reconstructions

Figure 4: **Image swapping**. Each row shows the result of combining the structure code of the leftmost image with the texture code of the top image (trained on LSUN Church and Bedroom). Our model generates realistic images that preserve texture (e.g., material of the building, or the bedsheet pattern) and structure (outline of objects).

Method	Runtime (sec) (↓)	Human Perceptual Study (AMT Fooling Rate) (↑)			
		Church	FFHQ	Waterfall	**Average**
Swap Autoencoder (Ours)	**0.113**	**31.3±2.4**	**19.4±2.0**	**41.8±2.2**	**31.0±1.4**
Im2StyleGAN [1, 45]	990	8.5±2.1	3.9±1.1	12.8±2.4	8.4±1.2
StyleGAN2 [46]	192	24.3±2.2	13.8±1.8	35.3±2.4	24.4±1.4
STROTSS [51]	166	13.7±2.2	3.5±1.1	23.0±2.1	13.5±1.2
WCT^2 [85]	1.35	*27.9±2.3*	**22.3±2.0**	35.8±2.4	*28.6±1.3*

Table 1: **Realism of swap-generated images** We study how realistic our swap-generated swapped appear, compared to state-of-the-art generative modeling approaches (Im2StyleGAN and StyleGAN2) and stylization methods (STROTSS and WCT^2). We run a perceptual study, where each method/dataset is evaluated with 1000 human judgments. We **bold** the best result per column and ***bold+italicize*** methods that are within the statistical significance of the top method. Our method achieves the highest score across all datasets. Note that WCT^2 is a method tailored especially for photorealistic style transfer and is within the statistical significance of our method in the perceptual study. Runtime is reported for 1024×1024 resolution.

and quantitative measurement of reconstruction quality, using LPIPS [91] between the original and embedded images. Note that our method accurately preserves the doorway pattern (top) and facial features (bottom) without blurriness. Averaged across datasets and on 5 of the 6 comparisons to the baselines, our method achieves *better reconstruction quality* than the baselines. An exception is on the Church dataset, where Im2StyleGAN obtains a better reconstruction score. Importantly, as our method is designed with test-time embedding in mind, it only requires a single feedforward pass, at least $1000\times$ faster than the baselines that require hundreds to thousands of optimization steps. Next, we investigate how *useful* the embedding is by exploring manipulations with the resulting code.

4.3 Swapping to produce image hybrids

In Figure 4, we show example hybrid images with our method, produced by combining structure and texture codes from different images. Note that the textures of the top row of images are consistently transferred; the sky, facade, and window patterns are mapped to the appropriate regions on the structure images on the churches, and similarly for the bedsheets.

Realism of image hybrids. In Table 1, we show results of comparison to existing methods. As well as generative modeling methods [1, 46, 45]. For image hybrids, we additionally compare with SOTA style transfer methods [51, 85], although they are not directly applicable for controllable editing by embedding images (Section 4.5). We run a human perceptual study, following the test setup used in [90, 35, 72]. A real and generated image are shown sequentially for one second each to Amazon Mechanical Turkers (AMT), who choose which they believe to be fake. We measure how often they fail to identify the fake. An algorithm generating perfectly plausible images would achieve a fooling

| Structure | Texture | StyleGAN2 | Im2StyleGAN | STROTSS | WCT² | Ours |
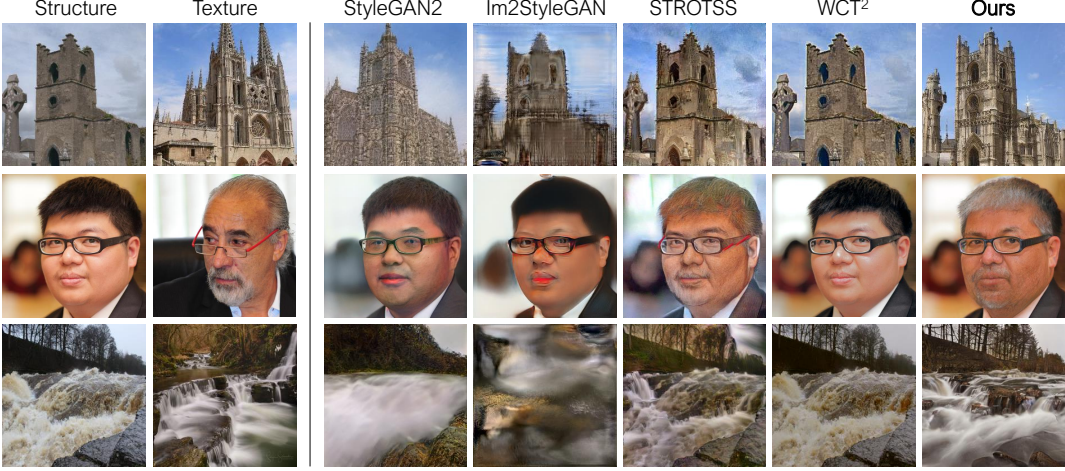
Figure 5: **Comparison of image hybrids.** Our approach generates realistic results that combine scene structure with elements of global texture, such as the shape of the towers (church), the hair color (portrait), and the long exposure (waterfall). Please see Appendix A for more comparisons.
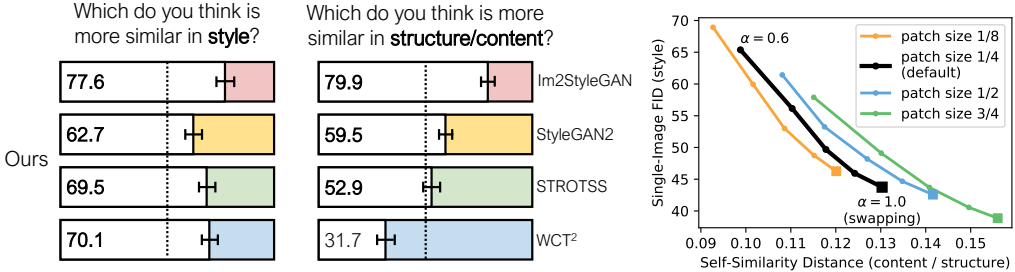

Figure 6: **Style and content**. **(Left)** Results of our perceptual study where we asked users on AMT to choose which image better reflects the "style" or "content" of a provided reference image, given two results (ours and a baseline). Our model is rated best for capturing style, and second-best for preserving content, behind WCT² [85], a photorealistic style transfer method. Most importantly, our method was rated strictly better in both style and content matching than both image synthesis models Im2StyleGAN [1, 45] and StyleGAN2 [46]. **(Right)** Using the self-similarity distance [51] and SIFID [72], we study variations of the co-occurrence discriminator's patch size in training with respect to the image size. As patch size increases, our model tends to make more changes in swapping (closer to the target style and further from input structure). In addition, we gradually interpolate the texture code, with interpolation ratio α, away from a full swapping $\alpha = 1.0$, and observe that the transition is smooth.

rate of 50%. We gather 15,000 judgments, 1000 for each algorithm and dataset. Our method achieves more realistic results across all datasets. The nearest competitor is the WCT² [85] method, which is designed for photorealistic style transfer. Averaged across the three datasets, our method achieves the highest fooling rate ($31.0\pm1.4\%$), with WCT² closely following within the statistical significance ($28.6\pm1.3\%$). We show qualitative examples in Figure 5.

Style and content. Next, we study how well the concepts of *content* and *style* are reflected in the structure and texture codes, respectively. We employ a Two-alternative Forced Choice (2AFC) user study to quantify the quality of image hybrids in content and style space. We show participants our result and a baseline result, with the style or content reference in between. We then ask a user which image is more similar in style, or content respectively. Such 2AFC tests were used to train the LPIPS perceptual metric [91], as well as to evaluate style transfer methods in [51]. As no true automatic perceptual function exists, human perceptual judgments remain the "gold standard" for evaluating image synthesis results [90, 35, 10, 72]. Figure 6 visualizes the result of 3,750 user judgments over four baselines and three datasets, which reveal that our method outperforms all baseline methods with statistical significance in style preservation. For content preservation, our method is only behind WCT², which is a photorealistic stylization method that makes only minor color modifications to the input. Most importantly, our method achieves the best performance with statistical significance in both style and content among models that can embed images, which is required for other forms of image editing.
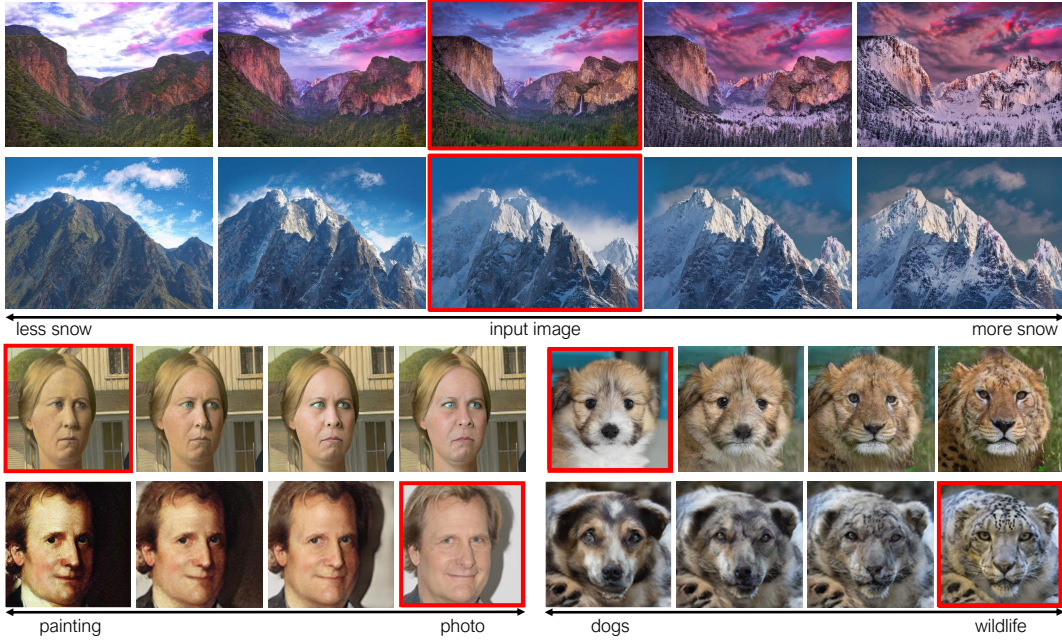
Figure 7: **Continuous interpolation**. **(top)** A manipulation vector for *snow* is discovered by taking mean difference between 10 user-collected photos of snowy and summer mountain. The vector is simply added to the texture code of the input image (red) with some gain. **(bottom)** Multi-domain, continuous transformation is achieved by applying the average vector difference between the texture codes of two domains, based on annotations from the training sets. We train on Portrait2FFHQ and AFHQ [12] datasets. See Appendix A for more results.

4.4   Analysis of our method

Next we analyze the behavior of our model using automated metrics. Self-similarity Distance [51] measures structural similarity in deep feature space based on the self-similarity map of ImageNet-pretrained network features. Single-Image FID [72] measures style similarity by computing the Fréchet Inception Distance (FID) between two feature distributions, each generated from a single image. SIFID is similar to Gram distance, a popular metric in stylization methods [18, 17], but differs by comparing the mean of the feature distribution as well as the covariance.

Specifically, we vary the size of cropped patches for the co-occurrence patch discriminator in training. In Figure 6 *(right)*, the max size of random cropping is varied from $1/8$ to $3/4$ of the image side length, including the default setting of $1/4$. We observe that as the co-occurrence discriminator sees larger patches, it enforces stronger constraint, thereby introducing more visual change in both style and content. Moreover, instead of full swapping, we gradually interpolate one texture code to the other. We observe that the SIFID and self-similarity distance both change gradually, in all patch settings. Such gradual visual change can be clearly observed in Figure 7, and the metrics confirm this.

4.5   Image editing via latent space operations

Even though no explicit constraint was enforced on the latent space, we find that modifications to the latent vectors cause smooth and predictable transformations to the resulting images. This makes such a space amenable to downstream editing in multiple ways. First, we find that our representation allows for controllable image manipulations by **vector arithmetic** in the latent space. Figure 7 shows that adding the same vector smoothly transforms different images into a similar style, such as gradually adding more snow *(top)*. Such vectors can be conveniently derived by taking the mean difference between the embeddings of two groups of images.

In a similar mechanism, the learned embedding space can also be used for **image-to-image translation** tasks (Figure 7), such as transforming paintings to photos. Image translation is achieved by applying the domain translation vector, computed as the mean difference between the two domains. Compared to most existing image translation methods, our method does not require that all images are labeled, and also allows for multi-domain, fine-grained control simply by modifying the vector magnitude and

members of the domain at test time. Finally, the design of the structure code $\mathbf{z}_s$ is directly amenable **local editing** operations, due to its spatial nature; we show additional results in Appendix A.

4.6 Interactive user interface for image editing

Based on the proposed latent space exploration methods, we built a sample user interface for creative user control over photographs. Figure 8 shows three editing modes that our model supports. Please see a demo video on our webpage. We demonstrate three operations: (1) **global style editing**: the texture code can be transformed by adding predefined manipulation vectors that are computed from PCA on the train set. Like GANSpace [21], the user is provided with knobs to adjust the gain for each manipulation vector. (2) **region editing**: the structure code can also be manipulated the same way of using PCA components, by treating each location as individual, controllable vectors. In addition, masks can be automatically provided to the user based on the self-similarity map at the location of interest to control the extent of structural manipulation. (3) **cloning**: the structure code can be directly edited using a brush that replaces the code from another part of the image, like the Clone Stamp tool of Photoshop.

UI with input image — brush stroke visualization — 1. remove road — 2. draw mountain

region editing with self-similarity mask — global style editing
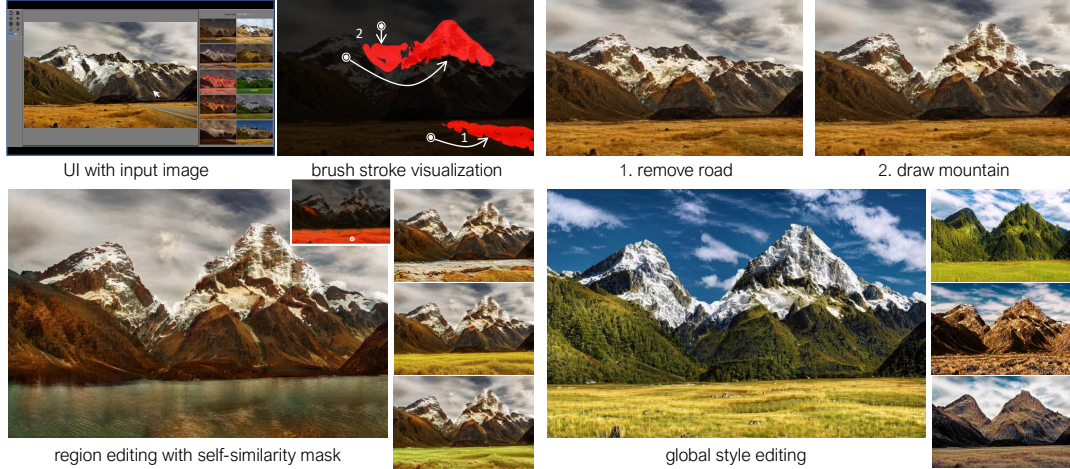
Figure 8: **Example Interactive UI. (top, cloning)** using an interactive UI, part of the image is "redrawn" by the user with a brush tool that extracts structure code from user-specified location. **(left, region editing)** the bottom region is transformed to lake, snow, or different vegetation by adding a manipulation vector to the structure codes of the masked region, which is auto-generated from the self-similarity map at the specified location. **(right, global style editing)** the overall texture and style can be changed using vector arithmetic with principal directions of PCA, controlled by the sliders on the right pane of the UI. (best viewed zoomed in)

5 Discussion

The main question we would like to address, is whether unconditional random image generation is required for high-quality image editing tasks. For such approaches, projection becomes a challenging operation, and intuitive disentanglement still remains a challenging question. We show that our method based on an auto-encoder model has a number of advantages over prior work, in that it can accurately embed high-resolution images in real-time, into an embedding space that disentangles texture from structure, and generates realistic output images with both swapping and vector arithmetic. We performed extensive qualitative and quantitative evaluations of our method on multiple datasets. Still, structured texture transfer remains challenging, such as the striped bedsheet of Figure 4. Furthermore, extensive analysis on the nature of disentanglement, ideally using reliable, automatic metrics will be beneficial as future work.

Broader Impact

From the sculptor's chisel to the painter's brush, tools for creative expression are an important part of human culture. The advent of digital photography and professional editing tools, such as Adobe Photoshop, has allowed artists to push creative boundaries. However, the existing tools are typically too complicated to be useful by the general public. Our work is one of the new generation of visual content creation methods that aim to democratize the creative process. The goal is to provide intuitive controls (see Section 4.6) for making a wider range of realistic visual effects available to non-experts.

While the goal of this work is to support artistic and creative applications, the potential misuse of such technology for purposes of deception – posing generated images as real photographs – is quite concerning. To partially mitigate this concern, we can use the advances in the field of image forensics [16], as a way of verifying the authenticity of a given image. In particular, Wang et al. [78] recently showed that a classifier trained to classify between real photographs and synthetic images generated by ProGAN [44], was able to detect fakes produced by other generators, among them, StyleGAN [45] and Style-GAN2 [46]. We take a pretrained model of [78] and report the detection rates on several datasets in Appendix C. Our swap-generated images can be detected with an average rate greater than 90%, and this indicates that our method shares enough architectural components with previous methods to be detectable. However, these detection methods do not work at 100%, and performance can degrade as the images are degraded in the wild (e.g., compressed, rescanned) or via adversarial attacks. Therefore, the problem of verifying image provenance remains a significant challenge to society that requires multiple layers of solutions, from technical (such as learning-based detection systems or authenticity certification chains), to social, such as efforts to increase public awareness of the problem, to regulatory and legislative.

Funding Disclosure

References

[1] Abdal, R., Qin, Y., Wonka, P.: Image2stylegan: How to embed images into the stylegan latent space? In: IEEE International Conference on Computer Vision (ICCV) (2019) 2, 5, 6, 7, 15, 19, 23

[2] Anokhin, I., Solovev, P., Korzhenkov, D., Kharlamov, A., Khakhulin, T., Silvestrov, A., Nikolenko, S., Lempitsky, V., Sterkin, G.: High-resolution daytime translation without domain labels. In: The IEEE Conference on Computer Vision and Pattern Recognition (CVPR) (June 2020) 1, 2, 3

[3] Asim, M., Shamshad, F., Ahmed, A.: Blind image deconvolution using deep generative priors. arXiv preprint arXiv:1802.04073 (2018) 2

[4] Bau, D., Strobelt, H., Peebles, W., Wulff, J., Zhou, B., Zhu, J.Y., Torralba, A.: Semantic photo manipulation with a generative image prior. ACM Transactions on Graphics (TOG) **38**(4), 1–11 (2019) 2

[5] Bau, D., Zhu, J.Y., Strobelt, H., Bolei, Z., Tenenbaum, J.B., Freeman, W.T., Torralba, A.: Gan dissection: Visualizing and understanding generative adversarial networks. In: International Conference on Learning Representations (ICLR) (2019) 2

[6] Bengio, Y.: Deep learning of representations: Looking forward. In: International Conference on Statistical Language and Speech Processing (2013) 3

[7] Brock, A., Donahue, J., Simonyan, K.: Large scale gan training for high fidelity natural image synthesis. In: International Conference on Learning Representations (ICLR) (2019) 5

[8] Brock, A., Lim, T., Ritchie, J.M., Weston, N.: Neural photo editing with introspective adversarial networks. In: International Conference on Learning Representations (ICLR) (2017) 2

[9] Chen, D., Yuan, L., Liao, J., Yu, N., Hua, G.: Stylebank: An explicit representation for neural image style transfer. In: Proceedings of the IEEE conference on computer vision and pattern recognition. pp. 1897–1906 (2017) 3

[10] Chen, Q., Koltun, V.: Photographic image synthesis with cascaded refinement networks. In: IEEE International Conference on Computer Vision (ICCV) (2017) 2, 7

[11] Chen, X., Duan, Y., Houthooft, R., Schulman, J., Sutskever, I., Abbeel, P.: Infogan: Interpretable representation learning by information maximizing generative adversarial nets. In: Advances in Neural Information Processing Systems (2016) 2, 3

[12] Choi, Y., Uh, Y., Yoo, J., Ha, J.W.: Stargan v2: Diverse image synthesis for multiple domains. In: Proceedings of the IEEE Conference on Computer Vision and Pattern Recognition (2020) 2, 5, 8, 15, 22

[13] Dinh, L., Sohl-Dickstein, J., Bengio, S.: Density estimation using real nvp. In: International Conference on Learning Representations (ICLR) (2017) 2, 3

[14] Dosovitskiy, A., Brox, T.: Generating images with perceptual similarity metrics based on deep networks. In: Advances in Neural Information Processing Systems (2016) 3

[15] Esser, P., Haux, J., Ommer, B.: Unsupervised robust disentangling of latent characteristics for image synthesis. In: Proceedings of the IEEE International Conference on Computer Vision. pp. 2699–2709 (2019) 2, 3

[16] Farid, H.: Photo forensics. MIT press (2016) 10

[17] Gatys, L., Ecker, A.S., Bethge, M.: Texture synthesis using convolutional neural networks. In: Advances in Neural Information Processing Systems (2015) 2, 4, 8

[18] Gatys, L.A., Ecker, A.S., Bethge, M.: Image style transfer using convolutional neural networks. In: IEEE Conference on Computer Vision and Pattern Recognition (CVPR) (2016) 3, 5, 8

[19] Goodfellow, I., Pouget-Abadie, J., Mirza, M., Xu, B., Warde-Farley, D., Ozair, S., Courville, A., Bengio, Y.: Generative adversarial nets. In: Advances in Neural Information Processing Systems (2014) 2, 3, 22

[20] Guérin, E., Digne, J., Galin, E., Peytavie, A., Wolf, C., Benes, B., Martinez, B.: Interactive example-based terrain authoring with conditional generative adversarial networks. ACM Transactions on Graphics (TOG) **36**(6) (2017) 2

[21] Härkönen, E., Hertzmann, A., Lehtinen, J., Paris, S.: Ganspace: Discovering interpretable gan controls. In: Advances in Neural Information Processing Systems (2020) 2, 9

[22] He, K., Zhang, X., Ren, S., Sun, J.: Deep residual learning for image recognition. In: IEEE Conference on Computer Vision and Pattern Recognition (CVPR) (2016) 5, 21

[23] He, M., Chen, D., Liao, J., Sander, P.V., Yuan, L.: Deep exemplar-based colorization. ACM Transactions on Graphics (TOG) **37**(4), 1–16 (2018) 2

[24] Heeger, D.J., Bergen, J.R.: Pyramid-based texture analysis/synthesis. In: Proceedings of the 22nd annual conference on Computer graphics and interactive techniques. pp. 229–238 (1995) 2

[25] Hertzmann, A., Jacobs, C.E., Oliver, N., Curless, B., Salesin, D.H.: Image analogies. In: ACM Transactions on Graphics (TOG) (2001) 3

[26] Heusel, M., Ramsauer, H., Unterthiner, T., Nessler, B., Hochreiter, S.: GANs trained by a two time-scale update rule converge to a local Nash equilibrium. In: Advances in Neural Information Processing Systems (2017) 20

[27] Higgins, I., Matthey, L., Pal, A., Burgess, C., Glorot, X., Botvinick, M., Mohamed, S., Lerchner, A.: beta-vae: Learning basic visual concepts with a constrained variational framework. In: International Conference on Learning Representations (ICLR) (2017) 3

[28] Hinton, G.E., Salakhutdinov, R.R.: Reducing the dimensionality of data with neural networks. Science **313**(5786), 504–507 (2006) 3

[29] Hong, S., Yan, X., Huang, T.S., Lee, H.: Learning hierarchical semantic image manipulation through structured representations. In: Advances in Neural Information Processing Systems (NeurIPS) (2018) 1

[30] Hu, Q., Szabó, A., Portenier, T., Favaro, P., Zwicker, M.: Disentangling factors of variation by mixing them. In: IEEE Conference on Computer Vision and Pattern Recognition (CVPR) (2018) 2

[31] Huang, X., Liu, M.Y., Belongie, S., Kautz, J.: Multimodal unsupervised image-to-image translation. European Conference on Computer Vision (ECCV) (2018) 2

[32] Huh, M., Liu, A., Owens, A., Efros, A.A.: Fighting fake news: Image splice detection via learned self-consistency. In: European Conference on Computer Vision (ECCV) (2018) 4

[33] Iizuka, S., Simo-Serra, E., Ishikawa, H.: Globally and locally consistent image completion. ACM Transactions on Graphics (TOG) **36**(4), 107 (2017) 2

[34] Ioffe, S., Szegedy, C.: Batch normalization: Accelerating deep network training by reducing internal covariate shift. In: International Conference on Machine Learning (ICML) (2015) 21

[35] Isola, P., Zhu, J.Y., Zhou, T., Efros, A.A.: Image-to-image translation with conditional adversarial networks. In: IEEE Conference on Computer Vision and Pattern Recognition (CVPR) (2017) 1, 2, 6, 7

[36] Isola, P., Zoran, D., Krishnan, D., Adelson, E.H.: Learning visual groups from co-occurrences in space and time. arXiv preprint arXiv:1511.06811 (2015) 4

[37] Jahanian, A., Chai, L., Isola, P.: On the"steerability" of generative adversarial networks. In: International Conference on Learning Representations (ICLR) (2020) 5

[38] Jha, A.H., Anand, S., Singh, M., Veeravasarapu, V.: Disentangling factors of variation with cycle-consistent variational auto-encoders. In: European Conference on Computer Vision (ECCV) (2018) 2, 3

[39] Johnson, J., Alahi, A., Fei-Fei, L.: Perceptual losses for real-time style transfer and super-resolution. In: European Conference on Computer Vision (ECCV) (2016) 3

[40] Julesz, B.: Visual pattern discrimination. IRE transactions on Information Theory **8**(2), 84–92 (1962) 2, 4

[41] Julesz, B.: Textons, the elements of texture perception, and their interactions. Nature **290**(5802), 91–97 (1981) 2

[42] Julesz, B., Gilbert, E.N., Shepp, L.A., Frisch, H.L.: Inability of humans to discriminate between visual textures that agree in second-order statistics—revisited. Perception **2**(4), 391–405 (1973) 2, 4

[43] Karacan, L., Akata, Z., Erdem, A., Erdem, E.: Manipulating attributes of natural scenes via hallucination. arXiv preprint arXiv:1808.07413 (2018) 1

[44] Karras, T., Aila, T., Laine, S., Lehtinen, J.: Progressive growing of gans for improved quality, stability, and variation. In: International Conference on Learning Representations (ICLR) (2018) 10, 23

[45] Karras, T., Laine, S., Aila, T.: A style-based generator architecture for generative adversarial networks. In: IEEE Conference on Computer Vision and Pattern Recognition (CVPR) (2019) 2, 3, 5, 6, 7, 10, 15, 19, 22, 23

[46] Karras, T., Laine, S., Aittala, M., Hellsten, J., Lehtinen, J., Aila, T.: Analyzing and improving the image quality of stylegan. IEEE Conference on Computer Vision and Pattern Recognition (CVPR) (2020) 2, 3, 4, 5, 6, 7, 10, 15, 19, 21, 22, 23

[47] Kazemi, H., Iranmanesh, S.M., Nasrabadi, N.: Style and content disentanglement in generative adversarial networks. In: 2019 IEEE Winter Conference on Applications of Computer Vision (WACV). pp. 848–856. IEEE (2019) 2

[48] Kim, H., Mnih, A.: Disentangling by factorising. In: International Conference on Machine Learning (ICML) (2018) 3

[49] Kingma, D.P., Ba, J.: Adam: A method for stochastic optimization. In: International Conference on Learning Representations (ICLR) (2015) 22

[50] Kingma, D.P., Welling, M.: Auto-encoding variational bayes. In: International Conference on Learning Representations (ICLR) (2014) 2, 3

[51] Kolkin, N., Salavon, J., Shakhnarovich, G.: Style transfer by relaxed optimal transport and self-similarity. In: IEEE Conference on Computer Vision and Pattern Recognition (CVPR) (2019) 5, 6, 7, 8, 15, 19, 20

[52] Kotovenko, D., Sanakoyeu, A., Lang, S., Ommer, B.: Content and style disentanglement for artistic style transfer. In: IEEE International Conference on Computer Vision (ICCV) (2019) 3

[53] Larsson, G., Maire, M., Shakhnarovich, G.: Learning representations for automatic colorization. In: European Conference on Computer Vision (ECCV) (2016) 2

[54] Lee, H.Y., Tseng, H.Y., Huang, J.B., Singh, M.K., Yang, M.H.: Diverse image-to-image translation via disentangled representation. In: European Conference on Computer Vision (ECCV) (2018) 3

[55] Li, Y., Liu, M.Y., Li, X., Yang, M.H., Kautz, J.: A closed-form solution to photorealistic image stylization. In: European Conference on Computer Vision (ECCV) (2018) 3

[56] Lin, J., Chen, Z., Xia, Y., Liu, S., Qin, T., Luo, J.: Exploring explicit domain supervision for latent space disentanglement in unpaired image-to-image translation. IEEE Transactions on Pattern Analysis and Machine Intelligence (TPAMI) (2019) 3

[57] Lin, T.Y., Maji, S.: Visualizing and understanding deep texture representations. In: Proceedings of the IEEE conference on computer vision and pattern recognition. pp. 2791–2799 (2016) 2

[58] Liu, G., Reda, F.A., Shih, K.J., Wang, T.C., Tao, A., Catanzaro, B.: Image inpainting for irregular holes using partial convolutions. In: European Conference on Computer Vision (ECCV) (2018) 1, 2

[59] Liu, M.Y., Huang, X., Mallya, A., Karras, T., Aila, T., Lehtinen, J., Kautz, J.: Few-shot unsupervised image-to-image translation. In: IEEE International Conference on Computer Vision (ICCV) (2019) 2

[60] Liu, Z., Luo, P., Wang, X., Tang, X.: Deep learning face attributes in the wild. In: IEEE International Conference on Computer Vision (ICCV) (2015) 22

[61] Luan, F., Paris, S., Shechtman, E., Bala, K.: Deep photo style transfer. In: IEEE Conference on Computer Vision and Pattern Recognition (CVPR) (2017) 3

[62] Mathieu, M.F., Zhao, J.J., Zhao, J., Ramesh, A., Sprechmann, P., LeCun, Y.: Disentangling factors of variation in deep representation using adversarial training. In: Advances in Neural Information Processing Systems (2016) 2, 3

[63] Mescheder, L., Geiger, A., Nowozin, S.: Which training methods for gans do actually converge? In: International Conference on Machine Learning (ICML) (2018) 22

[64] Park, T., Liu, M.Y., Wang, T.C., Zhu, J.Y.: Semantic image synthesis with spatially-adaptive normalization. In: IEEE Conference on Computer Vision and Pattern Recognition (CVPR) (2019) 1, 2

[65] Pathak, D., Krahenbuhl, P., Donahue, J., Darrell, T., Efros, A.A.: Context encoders: Feature learning by inpainting. In: IEEE Conference on Computer Vision and Pattern Recognition (CVPR) (2016) 1, 2

[66] Perarnau, G., van de Weijer, J., Raducanu, B., Álvarez, J.M.: Invertible conditional gans for image editing. In: NIPS Workshop on Adversarial Training (2016) 2

[67] Pidhorskyi, S., Adjeroh, D.A., Doretto, G.: Adversarial latent autoencoders. In: Proceedings of the IEEE Computer Society Conference on Computer Vision and Pattern Recognition (CVPR) (2020) 3

[68] Portenier, T., Hu, Q., Szabó, A., Bigdeli, S.A., Favaro, P., Zwicker, M.: Faceshop: Deep sketch-based face image editing. ACM Transactions on Graphics (TOG) **37**(4) (2018) 2

[69] Portilla, J., Simoncelli, E.P.: A parametric texture model based on joint statistics of complex wavelet coefficients. International journal of computer vision **40**(1), 49–70 (2000) 2, 4

[70] Salakhutdinov, R., Hinton, G.: Deep boltzmann machines. In: Artificial intelligence and statistics. pp. 448–455 (2009) 2

[71] Sangkloy, P., Lu, J., Fang, C., Yu, F., Hays, J.: Scribbler: Controlling deep image synthesis with sketch and color. In: IEEE Conference on Computer Vision and Pattern Recognition (CVPR) (2017) 2

[72] Shaham, T.R., Dekel, T., Michaeli, T.: Singan: Learning a generative model from a single natural image. In: IEEE International Conference on Computer Vision (ICCV) (2019) 2, 6, 7, 8, 20

[73] Shocher, A., Bagon, S., Isola, P., Irani, M.: Ingan: Capturing and remapping the" dna" of a natural image. In: IEEE International Conference on Computer Vision (ICCV) (2019) 2

[74] Singh, K.K., Ojha, U., Lee, Y.J.: Finegan: Unsupervised hierarchical disentanglement for fine-grained object generation and discovery. In: IEEE Conference on Computer Vision and Pattern Recognition (CVPR) (2019) 2, 3

[75] Tenenbaum, J.B., Freeman, W.T.: Separating style and content with bilinear models. Neural computation **12**(6), 1247–1283 (2000) 2, 3

[76] Ulyanov, D., Lebedev, V., Vedaldi, A., Lempitsky, V.: Texture networks: Feed-forward synthesis of textures and stylized images. In: International Conference on Machine Learning (ICML) (2016) 3

[77] Ulyanov, D., Vedaldi, A., Lempitsky, V.: Instance normalization: The missing ingredient for fast stylization. arXiv preprint arXiv:1607.08022 (2016) 21

[78] Wang, S.Y., Wang, O., Zhang, R., Owens, A., Efros, A.A.: Cnn-generated images are surprisingly easy to spot... for now. In: IEEE Conference on Computer Vision and Pattern Recognition (CVPR) (2020) 10, 23

[79] Wang, T.C., Liu, M.Y., Zhu, J.Y., Tao, A., Kautz, J., Catanzaro, B.: High-resolution image synthesis and semantic manipulation with conditional gans. In: IEEE Conference on Computer Vision and Pattern Recognition (CVPR) (2018) 1, 2

[80] Wu, W., Cao, K., Li, C., Qian, C., Loy, C.C.: Disentangling content and style via unsupervised geometry distillation. arXiv preprint arXiv:1905.04538 (2019) 2

[81] Xian, W., Sangkloy, P., Agrawal, V., Raj, A., Lu, J., Fang, C., Yu, F., Hays, J.: Texturegan: Controlling deep image synthesis with texture patches. In: IEEE Conference on Computer Vision and Pattern Recognition (CVPR) (2018) 2, 4

[82] Xing, X., Han, T., Gao, R., Zhu, S.C., Wu, Y.N.: Unsupervised disentangling of appearance and geometry by deformable generator network. In: IEEE Conference on Computer Vision and Pattern Recognition (CVPR) (2019) 2

[83] Yang, C., Lu, X., Lin, Z., Shechtman, E., Wang, O., Li, H.: High-resolution image inpainting using multi-scale neural patch synthesis. In: IEEE Conference on Computer Vision and Pattern Recognition (CVPR) (2017) 2

[84] Yeh, R.A., Chen, C., Yian Lim, T., Schwing, A.G., Hasegawa-Johnson, M., Do, M.N.: Semantic image inpainting with deep generative models. In: IEEE Conference on Computer Vision and Pattern Recognition (CVPR) (2017) 2

[85] Yoo, J., Uh, Y., Chun, S., Kang, B., Ha, J.W.: Photorealistic style transfer via wavelet transforms. In: IEEE International Conference on Computer Vision (ICCV) (2019) 3, 5, 6, 7, 15, 19

[86] Yu, F., Seff, A., Zhang, Y., Song, S., Funkhouser, T., Xiao, J.: Lsun: Construction of a large-scale image dataset using deep learning with humans in the loop. arXiv preprint arXiv:1506.03365 (2015) 2, 5, 15, 22

[87] Yu, J., Lin, Z., Yang, J., Shen, X., Lu, X., Huang, T.S.: Generative image inpainting with contextual attention. In: The IEEE Conference on Computer Vision and Pattern Recognition (CVPR) (June 2018) 1

[88] Yu, X., Chen, Y., Liu, S., Li, T., Li, G.: Multi-mapping image-to-image translation via learning disentanglement. In: Advances in Neural Information Processing Systems (NeurIPS) (2019) 2

[89] Zhang, R.: Making convolutional networks shift-invariant again. In: International Conference on Machine Learning (ICML) (2019) 21

[90] Zhang, R., Isola, P., Efros, A.A.: Colorful image colorization. In: European Conference on Computer Vision (ECCV) (2016) 2, 6, 7

[91] Zhang, R., Isola, P., Efros, A.A., Shechtman, E., Wang, O.: The unreasonable effectiveness of deep features as a perceptual metric. In: IEEE Conference on Computer Vision and Pattern Recognition (CVPR) (2018) 5, 6, 7

[92] Zhang, R., Zhu, J.Y., Isola, P., Geng, X., Lin, A.S., Yu, T., Efros, A.A.: Real-time user-guided image colorization with learned deep priors. ACM Transactions on Graphics (TOG) 9(4) (2017) 2

[93] Zhou, Y., Zhu, Z., Bai, X., Lischinski, D., Cohen-Or, D., Huang, H.: Non-stationary texture synthesis by adversarial expansion. ACM Transactions on Graphics (TOG) 37(4) (2018) 2

[94] Zhu, J.Y., Krähenbühl, P., Shechtman, E., Efros, A.A.: Generative visual manipulation on the natural image manifold. In: European Conference on Computer Vision (ECCV) (2016) 2, 5

[95] Zhu, J.Y., Park, T., Isola, P., Efros, A.A.: Unpaired image-to-image translation using cycle-consistent adversarial networks. In: IEEE International Conference on Computer Vision (ICCV) (2017) 1, 2

[96] Zhu, J.Y., Zhang, R., Pathak, D., Darrell, T., Efros, A.A., Wang, O., Shechtman, E.: Toward multimodal image-to-image translation. In: Advances in Neural Information Processing Systems (2017) 2

Appendix A   Results and Comparisons

A.1   Additional visual results

In Figure 1, 4, and 7 of the main paper, we have shown our results of swapping the texture and structure codes as well as manipulation results of the latent space. Here we show additional swapping and editing results.

Swapping. Here we show additional results of swapping on FFHQ (Figure 9), Mountains (Figure 12), and LSUN Church and Bedroom (Figure 14) dataset. For test images, the input images for the models trained on FFHQ (Figure 9, 10, and 11) and Mountains (Figure 12 and 13) are separately downloaded from `pixabay.com` using relevant keywords. The results on LSUN (Figure 14) are from the validation sets [86].

Editing. The latent space of our method can be used for image editing. For example, in Figure 11 and 13, we show the result of editing the texture code using an interactive UI that performs vector arithmetic using the PCA components. Editing the texture code results in changing global attributes like age, wearing glasses, lighting, and background in the FFHQ dataset (Figure 11), and time of day and grayscale in the Mountains dataset (Figure 13). On the other hand, editing the structure code can manipulate locally isolated attributes such as eye shape, gaze direction (Figure 10), or texture of the grass field (Figure 13). These results are generated by performing vector arithmetic in the latent space of the flattened structure code, masked by the region specified by the user in the UI, similar to region editing of Figure 8. In addition, the pond of Figure 13 is created by overwriting the structure code with the code of a lake from another image (cloning of Figure 8). More editing results of using the interactive UI can be found on our project webpage: `https://taesungp.github.io/SwappingAutoencoder`.

User-guided image translation. In Figure 16, we show the results of user-guided image translation, trained on Portrait2FFHQ and Animal Faces HQ [12]. For each dataset, the results are produced using the model trained on the mix of all domains and hence without any domain labels. By adjusting the gains on the principal components of the texture code with the interactive UI, the user controls the magnitude and style of translation. Interestingly, we found that the first principal axis of the texture code largely corresponds to the domain translation vector in the case of Portrait2FFHQ and AFHQ dataset, with the subsequent vectors controlling more fine-grained styles. Therefore, our model is suitable for the inherent multi-modal nature of image translation. For example, in Figure 16, the input cat and dog images are translated into six different plausible outputs.

A.2   Additional comparison to existing methods

In Table 2, we report the FIDs of the swapping results of our model and baselines on LSUN Church, FFHQ, and Waterfall datasets using the validation set. More visual comparison results that extend Figure 3 and 5 of the main paper are in Figure 15. Note that using FID to evaluate the results of this task is not sufficient, as it does not capture the relationship to input content and style images. For example, a low FID can be achieved simply by not making large changes to the input content image. Our model achieves the second-best FID, behind the photorealistic style transfer method WCT^2 [85]. However, the visual results of Figure 15 and human perceptual study of Figure 6 reveal that our method better captures the details of the reference style. In Table 3, we compare the FIDs of swapping on the training set with *unconditionally* generated StyleGAN and StyleGAN2 outputs. Note that randomly sampled images of StyleGAN and StyleGAN2 are not suitable for image editing, as it ignores the input image. The FID of swap-generated images of our method is placed between the FID of unconditionally generated StyleGAN and StyleGAN2 images.

Method	Church	FFHQ	Waterfall	Mean
Swap Autoencoder (Ours)	52.34	59.83	50.90	54.36
Im2StyleGAN [1, 45]	219.50	123.13	267.25	203.29
StyleGAN2 [46]	57.54	81.44	57.46	65.48
STROTSS [51]	70.22	92.19	108.41	83.36
WCT^2 [85]	35.65	39.02	35.88	36.85

Table 2: **FID of swapping on the validation set**. We compare the FIDs of content-style mixing on the validation sets. Note the utility of FID is limited in our setting, since it does not capture the quality of embedding or disentanglement. Our method achieves second-lowest FID, behind WCT^2 [85], a photorealistic style transfer method. Note that the values are not directly comparable to different datasets or to the training splits (Table 3), since the number of samples are different. Please see Figure 15 for visual results.

Method	Church	FFHQ	Waterfall
Swap Autoencoder (Ours)	3.91	3.48	3.04
StyleGAN [45]	4.21	4.40*	6.09
StyleGAN2 [46]	3.86*	2.84*	2.67

Table 3: **FID of swapping on the training set, in the context of unconditional GAN**. We compute the FID of swapped images on the training set, and compare it with FIDs of unconditionally generated images of Style-GAN [45] and StyleGAN2 [46]. The result conveys how much realism the swap-generated images convey. Note that randomly sampled images of StyleGAN [45] and StyleGAN2 [46] models are not suitable for image editing. Asterisk(*) denotes FIDs reported in the original papers.

Figure 9: **Swapping results of our FFHQ model**. The input photographs are collected from `pixabay.com`.

input   bigger eyes   gaze direction   more smile   5 o'clock shadow
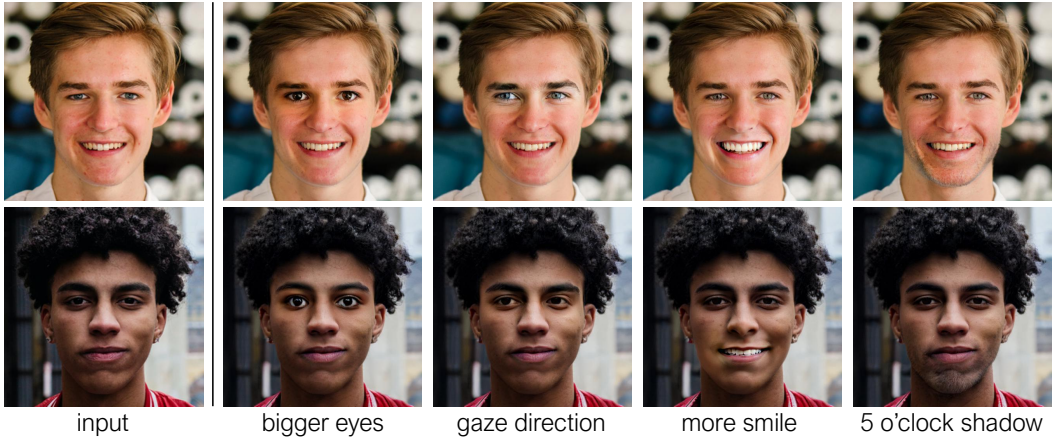
Figure 10: **Region editing**. The results are generated by performing vector arithmetic on the structure code. The vectors are discovered by a user with our UI, with each goal in mind.


input   age   glasses   lighting   background
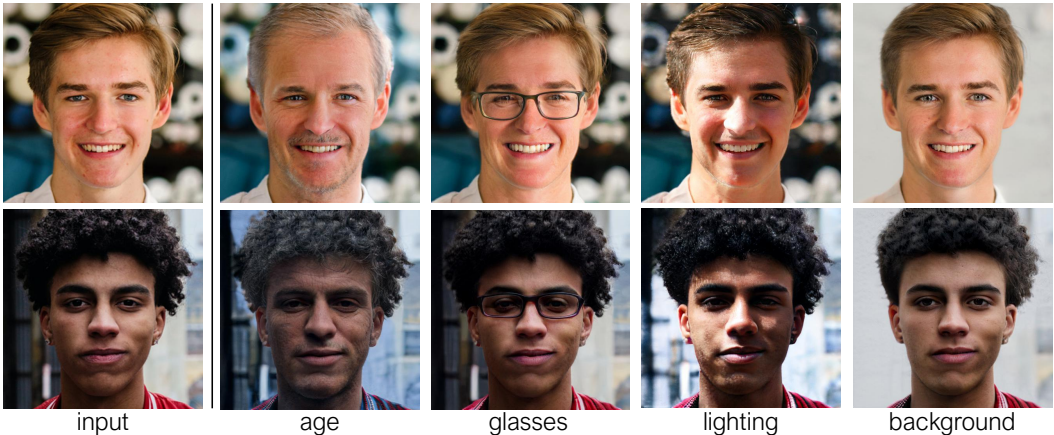
Figure 11: **Global editing**. The results are generated using vector arithmetic on the texture code. The vectors are discovered by a user with our UI, with each goal in mind.

16
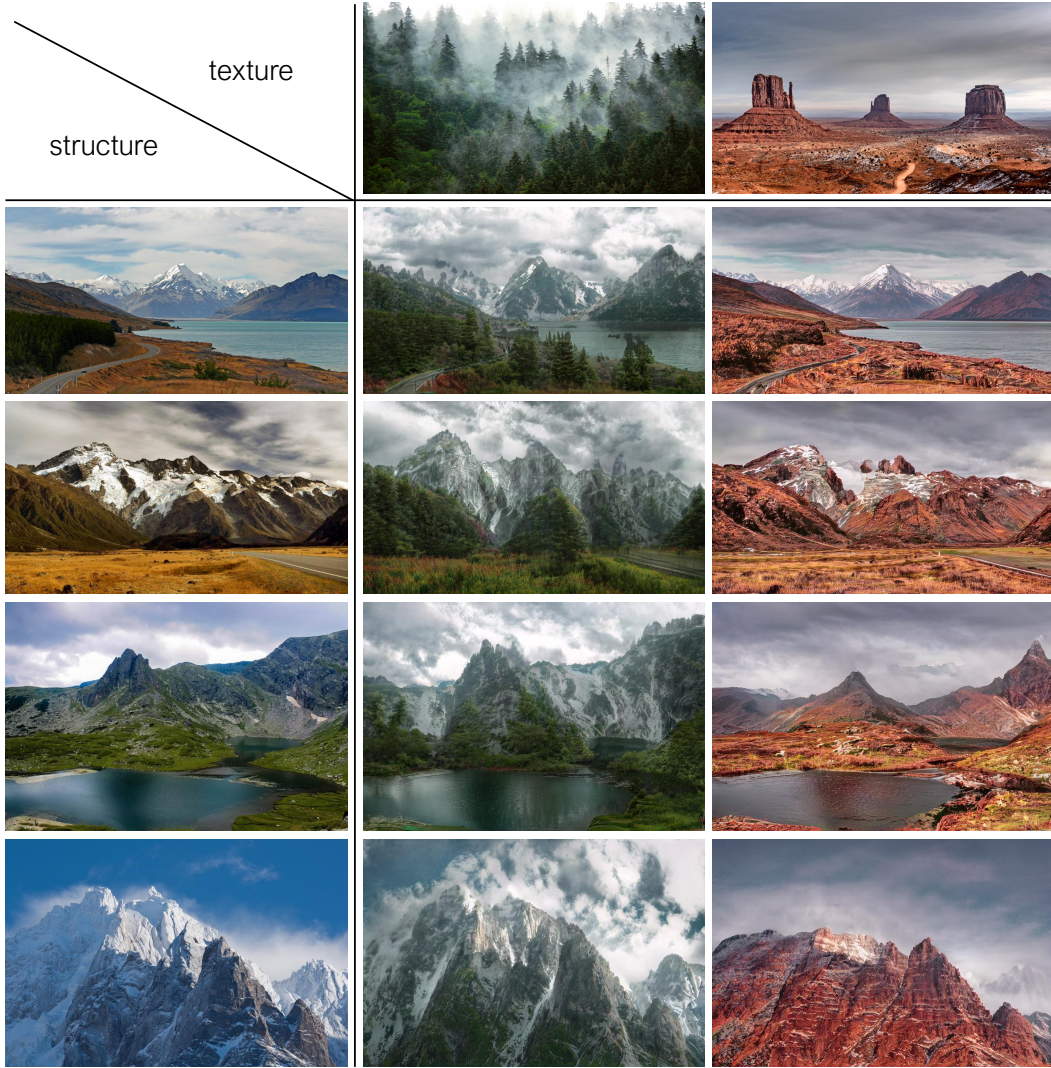
Figure 12: **Swapping results of our method trained on Flickr Mountains**. The model is trained and tested at 512px height.

Figure 13: **User editing results of our method trained on Flickr Mountains**. For the input image in red, the top and bottom rows show examples of editing the structure and texture code, respectively. Please refer to Figure 8 on how editing is performed. The image is of 1536×1020 resolution, using a model trained at 512px resolution.
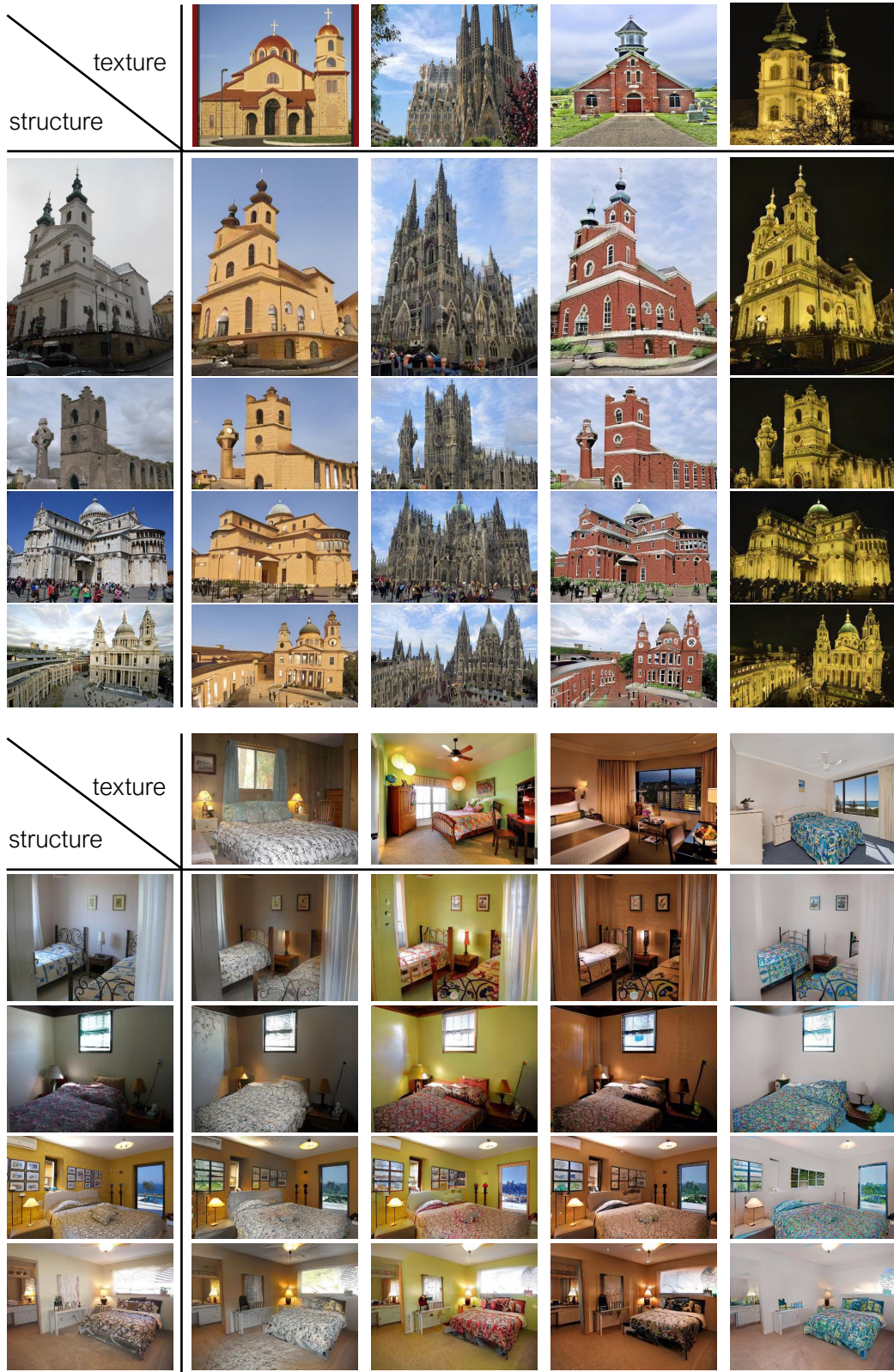
Figure 14: **Swapping results of LSUN** Churches (top) and Bedrooms (bottom) validation set. The model is trained with 256px-by-256px crops and tested at 256px resolution on the shorter side, keeping the aspect ratio.
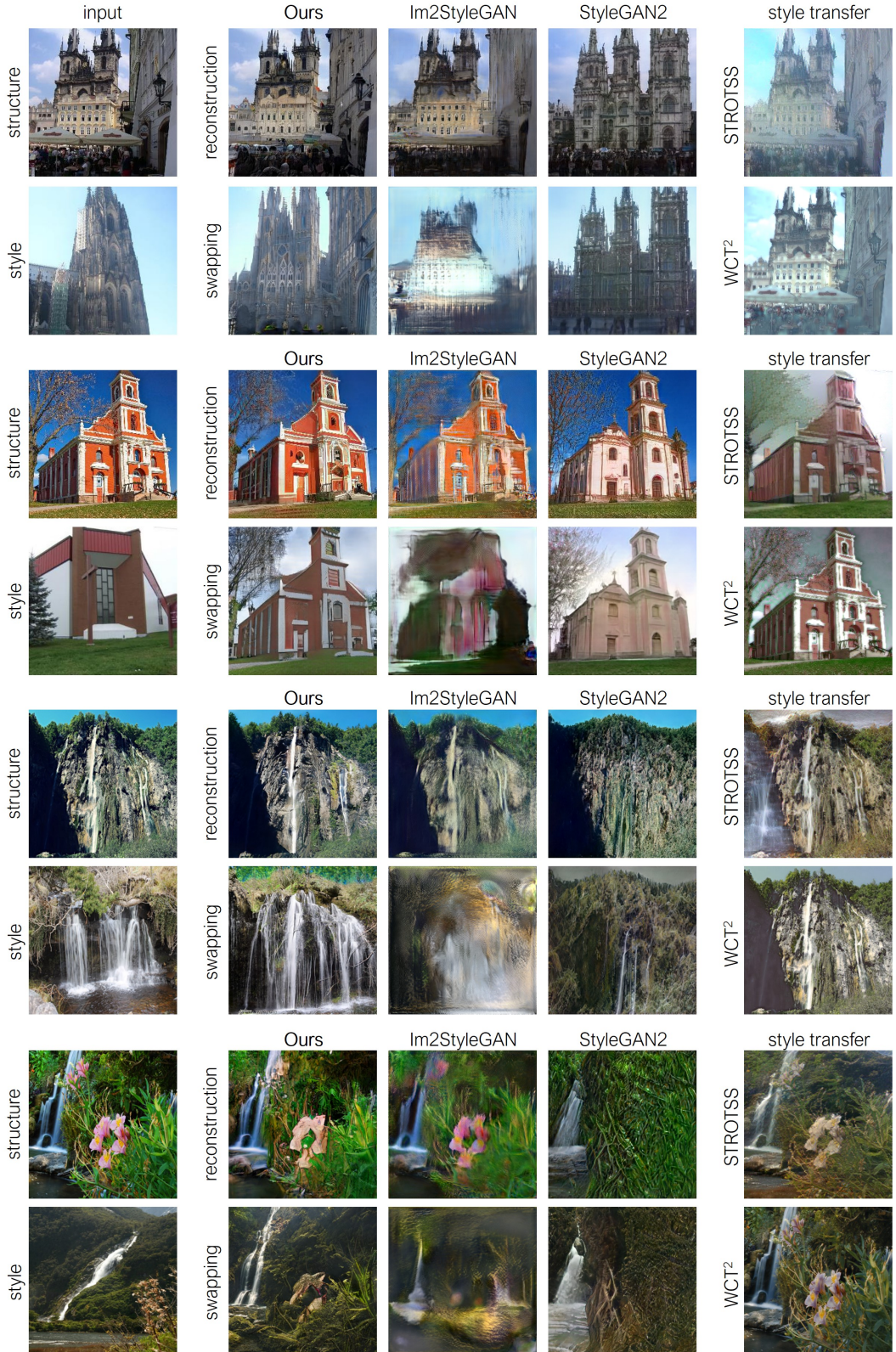
Figure 15: **Comparison to existing methods**. Random results on LSUN Churches and Flickr Waterfall are shown. In each block, we show both the reconstruction and swapping for ours, Im2StyleGAN [1, 45], and StyleGAN2 [46], as well as the style transfer results of STROTSS [51] and WCT[2] [85]. Im2StyleGAN has a low reconstruction error but performs poorly on the swapping task. StyleGAN2 generates realistic swappings, but fails to capture the input images faithfully. Both style transfer methods makes small changes to the input structure images.
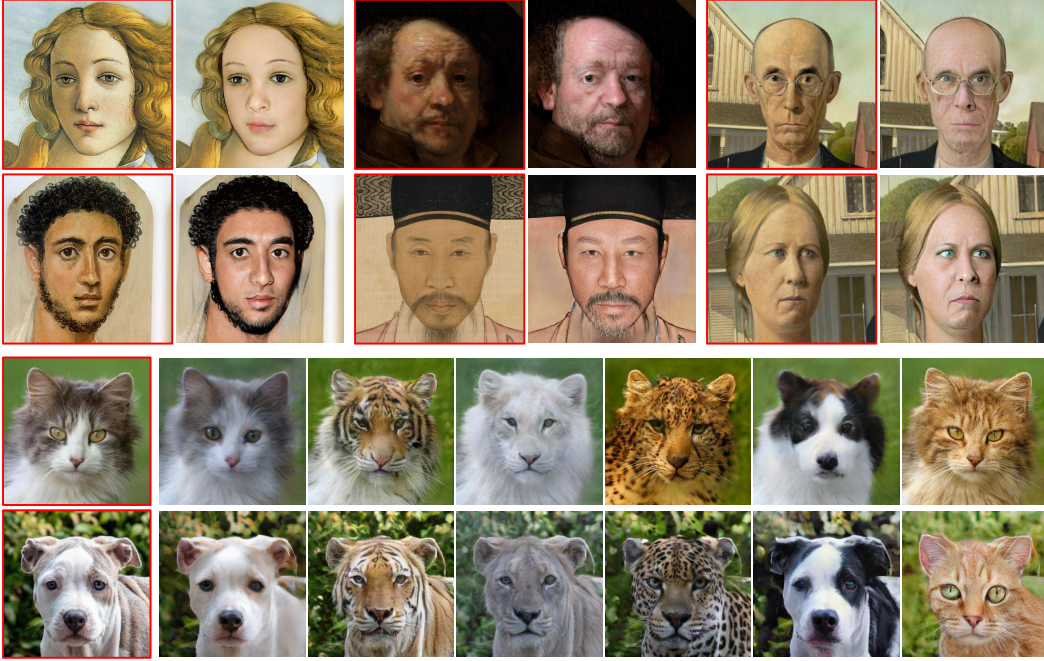
Figure 16: **User-guided image translation**. Using the interactive UI, the user controls the magnitude and style of the translated image. We show the edit results of turning paintings into photo (top) on the model trained on the Portrait2FFHQ dataset, and translating within the Animal Faces HQ dataset (bottom). The input images are marked in red. For the animal image translation, 6 different outputs are shown for the same input image.

A.3 Corruption study of Self-Similarity Distance and SIFID

In Figure 17, we validate our usage of Self-Similarity Matrix Distance [51] and Single-Image FID (SIFID) [72] as automated metrics for measuring distance in structure and style. Following FID [26], we study the change in both metrics under predefined corruptions. We find that the self-similarity distance shows a larger variation for image translation and rotation than blurring or adding white noise. In contrast, SIFID is more sensitive to blurring or white noise than translation or rotation. This confirms that the self-similarity captures structure, and SIFID captures style.
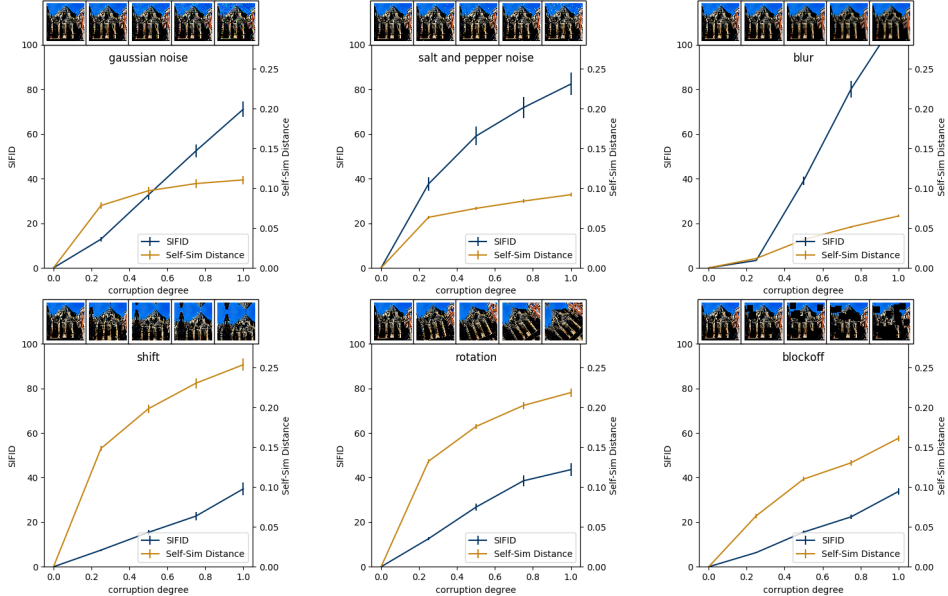

Figure 17: **Validating the Self-Similarity Matrix Distance and Single-Image FID**. We apply different types of corruptions and study the variation in the Self-Similarity Distance [51] and Single-Image FID [72]. SIFID shows higher sensitivity to overall style changes, such as Gaussian noise or blurring, than structural changes, such as shift and rotation. On the other hand, Self-Similarity Distance shows higher variation for structural changes. This empirically confirms our usage of the two metrics as measuring distance in structure and style.

Appendix B Implementation details

We show our architecture designs, additional training details, and provide information about our datasets.

B.1   Architecture

The **encoder** maps the input image to structure and texture codes, as shown in Figure 18 (left). For the structure code, the network consists of 4 downsampling residual blocks [22], followed by two convolution layers. For the texture code, the network branches off and adds 2 convolutional layers, followed by an average pooling (to completely remove spatial dimensions) and a dense layer. The asymmetry of the code shapes is designed to impose an inductive bias and encourage decomposition into orthogonal tensor dimensions. Given an 256×256 image, the structure code is of dimension $16 \times 16 \times 8$ (large spatial dimension), and texture code is of dimension $1 \times 1 \times 2048$ (large channel dimension).

The texture code is designed to be agnostic to positional information by using reflection padding or no padding ("valid") in the convolutional layers (rather than zero padding) followed by average pooling. On the other hand, each location of the structure code has a strong inductive bias to encode information in its neighborhood, due to its fully convolutional architecture and limited receptive field.

The **generator** maps the codes back to an image, as shown in Figure 18 (right). The network uses the structure code in the main branch, which consists of 4 residual blocks and 4 upsampling residual blocks. The texture code is injected using the weight modulation/demodulation layer from StyleGAN2 [46]. We generate the output image by applying a convolutional layer at the end of the residual blocks. This is different from the default setting of StyleGAN2, which uses an output skip, but more similar to the residual net setting of StyleGAN2 discriminator. Lastly, to enable isolated local editing, we avoid normalizations such as instance or batch normalization [77, 34].

The **discriminator** architecture is identical to StyleGAN2, except with no minibatch discrimination, to enable easier fine-tuning at higher resolutions with smaller batch sizes.

The **co-occurrence patch discriminator** architecture is shown in Figure 19 and is designed to determine if a patch in question ("real/fake patch") is from the same image as a set of reference patches. Each patch is first independently encoded with 5 downsampling residual blocks, 1 residual block, and 1 convolutional layer. The representations for the reference patches are averaged together and concatenated with the representation of the real/fake patch. The classification applies 3 dense layers to output the final prediction.

The detailed design choices of the layers in all the networks follow StyleGAN2 [46], including weight demodulation, antialiased bilinear down/upsampling [89], equalized learning rate, noise injection at every layer, adjusting variance of residual blocks by the division of $\sqrt{2}$, and leaky ReLU with slope 0.2.
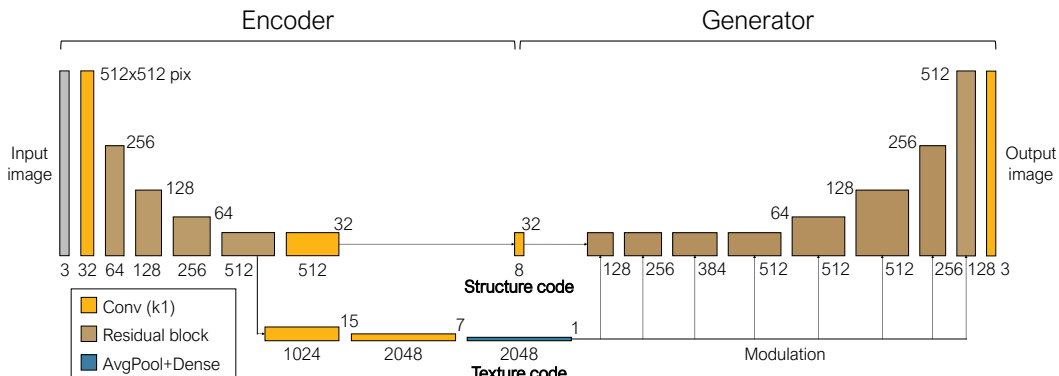

Figure 18: **Encoder and generator architecture**. The encoder network first applies 4 downsampling residual blocks [22] to produce an intermediate tensor, which is then passed to two separate branches, producing the structure code and texture code. The structure code is produced by applying 1-by-1 convolutions to the intermediate tensor. The texture code is produced by applying strided convolutions, average pooling, and then a dense layer. Given an $H \times H$ image, the shapes of the two codes are $H/16 \times H/16 \times 8$, and $1 \times 1 \times 2048$, respectively. The case for a 512×512 image is shown. To prevent the texture code from encoding positional information, we apply reflection padding for the residual blocks, and then no padding for the conv blocks. The generator consists of 4 residual blocks and then 4 upsampling residual blocks, followed by 1-by-1 convolution to produce an RGB image. The structure code is given in the beginning of the network, and the texture code is provided at every layer as modulation parameters. We use zero padding for the generator. The detailed architecture follows StyleGAN2 [46], including weight demodulation, bilinear upsampling, equalized learning rate, noise injection at every layer, adjusting variance of residual blocks by the division of $\sqrt{2}$, and leaky ReLU with slope 0.2.
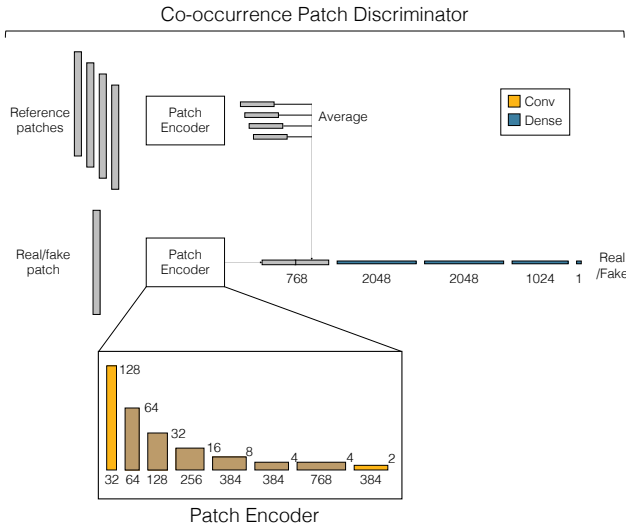
Figure 19: **Co-occurrence patch discriminator architecture**. The co-occurrence patch discriminator consists of the feature extractor, which applies 5 downsampling residual blocks, 1 residual block, and 1 convolutional layer with valid padding to each input patch, and the classifier, which concatenates the flattened features in channel dimension and then applies 3 dense layers to output the final prediction. Since the patches have random sizes, they are upscaled to the same size before passed to the co-occurrence discriminator. All convolutions use kernel size $3{\times}3$. Residual blocks use the same design as those of the image discriminator. For the reference patches, more than one patch is used, so the extracted features are averaged over the batch dimension to capture the aggregated distribution of the reference texture.

B.2 Training details

At each iteration, we sample a minibatch of size N and produce $N/2$ reconstructed images and $N/2$ hybrid images. The reconstruction loss is computed using $N/2$ reconstructed images. The loss for the image discriminator is computed on the real, reconstructed, and hybrid images, using the adversarial loss $\mathbb{E}[-\log(D(\mathbf{x}))] + \mathbb{E}[-\log(1-D(\mathbf{x}_{\text{fake}}))]$, where $\mathbf{x}$ and $\mathbf{x}_{\text{fake}}$ are real and generated (both reconstructed and hybrid) images, respectively. For the details of the GAN loss, we follow the setting of StyleGAN2 [46], including the non-saturating GAN loss [19] and lazy R1 regularization [63, 46]. In particular, R1 regularization is also applied to the co-occurrence patch discriminator. The weight for R1 regularization was 10.0 for the image discriminator (following the setting of [63, 46]) and 1.0 for the co-occurrence discriminator. Lastly, the co-occurrence patch discriminator loss is computed on random crops of the real and swapped images. The size of the crops are randomly chosen between $1/8$ and $1/4$ of the image dimensions for each side, and are then resized to $1/4$ of the original image. For each image (real or fake), 8 crops are made. For the query image (the first argument to D_{patch}), each crop is used to predict co-occurrence, producing $8N$ predictions at each iteration. For the reference image (the second argument to D_{patch}), the feature outputs are averaged before concatenated with the query feature. Both discriminators use the binary cross-entropy GAN loss.

We use ADAM [49] with 0.002 learning rate, $\beta_1 = 0.0$ and $\beta_2 = 0.99$. We use the maximum batch size that fits in memory on 8 16GB Titan V100 GPUs: 64 for images of $256{\times}256$ resolution, 16 for $512{\times}512$ resolution, and 16 for $1024{\times}1024$ resolution (with smaller network capacity). Note that only the FFHQ dataset was trained at $1024{\times}1024$ resolution; for the landscape datasets, we take advantage of the fully convolutional architecture and train with cropped images of size $512{\times}512$, and test on the full image. The weights on each loss term are simply set to be all 1.0 among the reconstruction, image GAN, and co-occurrence GAN loss.

B.3 Datasets

Here we describe our datasets in more detail.

LSUN Church [86] consists of 126,227 images of outdoor churches. The images are in the dataset are 256px on the short side. During training, $256{\times}256$ cropped images are used. A separate validation set of 300 images is used for comparisons against baselines.

LSUN Bedroom [86] consists of 3,033,042 images of indoor bedrooms. Like LSUN Church, the images are trained at $256{\times}256$ resolution. The results are shown with the validation set.

Flickr Faces HQ [45] consists of 70,000 high resolution aligned face images from `flickr.com`. Our model is initially trained at $512{\times}512$ resolution, and finetuned at 1024 resolution. The dataset designated 10,000 images for validation, but we train our model on the entire 70,000 images, following the practice of StyleGAN [45] and StyleGAN2 [46]. For evaluation, we used randomly selected 200 images from the validation set, although the models are trained with these images.

Animal Faces HQ [12] contains a total of 15,000 images equally split between cats, dogs, and a wildlife category. Our method is trained at $256{\times}256$ resolution on the combined dataset without domain labels. The results are shown with a separate validation set.

Portrait2FFHQ consists of FFHQ [45] and a newly collected 19,863 portrait painting images from `wikiart.org`. The model is trained at $512{\times}512$ resolution on the combined dataset. The results of the paper are generated from separately collected sample paintings. We did not check if the same painting belongs in the training set. The test photographs are from CelebA [60]. All images are aligned to match the facial landmarks of FFHQ dataset.

Flickr Waterfall is a newly collected dataset of 90,345 waterfall images. The images are downloaded from the user group "Waterfalls around the world" on `flickr.com`. The validation set is 399 images collected from the user group "*Waterfalls*". Our model is trained at 256×256 resolution.

Flickr Mountains is a newly collected dataset of 517,980 mountain images from Flickr. The images are downloaded from the user group "Mountains Anywhere" on `flickr.com`. For testing, separately downloaded sample images were used. Our model is trained at 512×512 resolution.

Appendix C   Detectability of Generated Images

To partially mitigate the concern of misusing our method as a tool for generating deceiving images, we see if a fake image detector can be applied to the images produced by our method. We run the off-the-shelf detector from [78], specifically, the Blur+JPEG(0.5) variant on the full, uncropped result images from this paper, and evaluate whether they are correctly classified as "synthesized". The results are shown in Table 4. For the most sensitive category, FFHQ faces, both previous generative models and our method have high detectability. We observe similar behavior, albeit with some drop-off on less sensitive categories of "church" and "waterfall".

Method	Task	Dataset			
		Church	FFHQ	Waterfall	Average
Im2StyleGAN [1, 45]	reconstruct	99.3	100.0	92.4	97.2
	swap	100.0	100.0	97.7	99.2
StyleGAN2 [46]	reconstruct	99.7	100.0	94.4	98.0
	swap	99.8	100.0	96.6	98.8
Swap Autoencoder (Ours)	reconstruct	93.6	95.6	73.9	87.7
	swap	96.6	94.7	80.4	90.5

Table 4: **Detectability.** We run the CNN-generated image detector from Wang et al. [78] and report average precision (AP); chance is 50%. The CNN classifier is trained from ProGAN [44], the predecessor to StyleGAN [45]. Because our method shares architectural components, a classifier trained to detect a different method can also generalize to ours, with some dropoff, especially for the waterfall class. Notably, the performance on FFHQ faces remains high. However, performance is not reliably at 100% across all methods, indicating that future detection methods could potentially benefit from training on our method.

Appendix D   Changelog

v1 Initial preprint release.

v2 Revised Introduction, reorganized Broader Impact, and added new references. NeurIPS 2020 Camera Ready.